Journal of the Mechanical Behavior of Biomedical Materials 78 (2018) 266–272

Contents lists available at ScienceDirect

Journal of the Mechanical Behavior of Biomedical Materials

journal homepage: www.elsevier.com/locate/jmbbm

Effect of wetting case and softness on adhesion of bioinspired micropatterned surfaces

Meng Li[a], Jun Xie[a], Qingwen Dai[a,b], Wei Huang[a,b], Xiaolei Wang[a,b,*]

[a] College of Mechanical & Electrical Engineering, Nanjing University of Aeronautics & Astronautics, Nanjing 210016, China
[b] Jiangsu Key Laboratory of Precision and Micro-Manufacturing Technology, Nanjing 210016, China

ARTICLE INFO

Keywords:
Amphibian
Wet adhesion
Hexagonal pillar
Softness
Wetting case

ABSTRACT

Inspired by the adhesive ability of amphibian toe-pads, polydimethylsiloxane (PDMS) hexagonal pillar arrayed surfaces with varying softness are fabricated, and their adhesion behaviors in the non-wetting, mostly wetting and totally wetting cases are throughly investigated. Experimental results demonstrate that under a totally wetting case, i.e. the biological toe-pad-like case, besides the long-range capillary force, a short-range interaction caused by close contact plays a significant role for adhesion. Compared with unpatterned surface, hexagonal pillar patterns can lead to a remarkable improvement in both short- and long-range contribution for wet adhesion. Meanwhile, the surface softness performs a beneficial character in the short-range contribution for the adhesion of micropillars. Considering the fact that the soft microstructure and the almost totally wetting case (low surface tension of secretion and high surface energy of epidermis) on the pads of nature species, it is reasonable to suggest that these evolutions are in favor for wet attachments.

1. Introduction

The amphibians such as tree frogs, torrent frogs and newts are remarkable in their ability of attaching and climbing in wet environments without falling (Barnes, 1999; Barnes et al., 2002; Drotlef et al., 2014; Endlein et al., 2013; Huang and Wang, 2013; Wang et al., 2016). This extraordinary ability is widely believed to be a result of the specific topography on their toe-pads, and massive scientific interest has be aroused over the past decade (Barnes et al., 2006; Barnes, 1999; Federle et al., 2006; Hanna and Barnes, 1991). Unlike the hairy tissue of geckos, the toe-pads of above amphibians are usually featured by a polygonal micro-structure of epidermal cells separated by mucus-filled channels (Barnes et al., 2013, 2002; Federle et al., 2006; Green, 1979; Green and Simon, 1986). Though the mechanism underlying natural wet attachments is still not fully clear, acquired experimental evidence suggests that these tailor-made polygonal patterns can allow the toe-pads to expel fluid out of the contact area between the pad epidermis and the substrate to achieve the “close contact” situation, and a boundary friction happens when a shear load is applied (Federle et al., 2006; Lorenz and Persson, 2011; Persson, 2007). These characteristics can significantly enhance the attachment forces of toe-pads on wet surfaces.

Abundant researches have demonstrated and characterized the high friction properties of bioinspired polygonal micropillars in wet sliding (Drotlef et al., 2013; Fischer et al., 2016; Huang and Wang, 2013; Iturri et al., 2015; Li et al., 2015; Roshan et al., 2011; Varenberg and Gorb, 2009). However, considering the various attaching modes of amphibians in nature, the adhesion force is also an important role for wet attachments. For example, tree-frogs can not only climb or attach slippery slopes but also hang upside down on wet leaves without falling. Barnes *et al.* early measured this considerable adhesive interaction on tree-frog toe-pads (about 1.2 mN mm^{-2}), and attributed it to capillary and viscous forces (Stefan adhesion) (Barnes, 1999, 2007; Hanna and Barnes, 1991). Federle et al. (2006) pointed out that the film between the pad and the substrate was extremely thin (mostly less than 35 nm), and this “close contact” played a positive role for wet attachments. Recently, Drotlef et al. (2013) carried out a pioneering adhesive study on tree-frog like micro-patterned PDMS surfaces with Young's modulus about 2 MPa. They found that the not viscous forces but capillary forces (a long-range attractive interaction) make main contribution for wet adhesion in a hydrophilic case (contact angle (CA) = 10°). However, considering biological adhesive toe-pads, there are another two facts that might be ignored in previous studies. First, the secreted mucus can widely spread on toe-pads due to its low surface tension, nearly presenting a totally wetting case (CA = 0°) (Drotlef et al., 2013; Federle et al., 2006; Persson, 2007). And next, as reported by Barnes (2007), Barnes et al. (2011) and (Scholz et al., 2009) the surface of biological toe-pads is extremely soft and malleable with a low Young modulus of approximately 4–40 kPa. Therefore, does the wetting

* Corresponding author at: College of Mechanical & Electrical Engineering, Nanjing University of Aeronautics & Astronautics, Nanjing 210016, China.
E-mail address: wxl@nuaa.edu.cn (X. Wang).

https://doi.org/10.1016/j.jmbbm.2017.11.036
Received 26 June 2017; Received in revised form 24 October 2017; Accepted 21 November 2017
Available online 22 November 2017
1751-6161/

case or surface softness have an influence on the wet adhesion of toe-pads? If so, how do the soft micropillars behave for adhesion in different wetting case, and what is the role of softness on micropillars for wet adhesion? To date, little research has been conducted to comprehend the wet adhesion on these aspects.

In this study, very soft hexagonal micropillar patterned surfaces were fabricated with a modified PDMS. Water, sodium dodecyl sulfate solution and dimethyl silicon oil were employed to achieve three different wetting cases (non-wetting case, mostly wetting case, totally wetting case) on PDMS surfaces. Then adhesion properties of micro-patterned surfaces to a silica glass probe were studied in different wetting cases. Moreover, the effects of softness on micropatterns on wet adhesion forces were assessed and analyzed.

2. Materials and methods

2.1. Mold preparation

Silica glasses were ultrasonically cleaned by acetone, ethyl alcohol and deionized water. Before lithographic processing, the wafers were rinsed with acetone and blown dry with nitrogen. An AZ P4620 photoresist is spun on these wafers at 2500 rpm for 8.5 μm film, followed by 2 min of soft baking at 100 °C. An optical lithography writer (Durham, Britain) were used to expose with 10 × 10 mm^2 fields and then the film was developed in AZ 400 K of 1:4 for molds.

2.2. Patterned surface preparation

PDMS (Sylgard 184, Dow Corning) was mixed with a prepolymer to cross-linker ratio of 10:1. The soft patterned surfaces were fabricated by filling a low viscosity dimethyl silicon oil (PMX-200, viscosity 10cs, Dow Corning) into the PDMS. The filled silicon oil molecules will stretch the crosslinked network of PDMS to lower the hardness and elasticity modulus of material (Fig. 1a). In this paper, the filling ratios (r) of dimethyl silicon oil were 0.5:1, 1:1 and 1.5:1 to the prepolymer of PDMS. All mixed liquids were degassed in a desiccator until no bubbles and cured in an oven for 12 h at 70 °C. After demoulding, samples were characterized using white-light interferometry (Bruker, USA) and digital microscope (Keyence, Japan). The side length of hexagonal pillars was 15 μm, the side distance was 7 μm and the height was 8.5 μm, as shown Fig. 1b.

2.3. Elastic modulus and hardness measurements

The elastic modulus of flat surfaces was measured using a custom-built equipment consisting of a tungsten steel pin with a flat tip (1 mm diameter, Young's modulus of 7.2 × 10^{11} Pa) mounted at the end of a cantilever (Supplementary material, Fig. S1) (Li et al., 2017). The operational process was similar to a typical elastic modulus test on nanoindentor. The preload of initial indentation on the surface was 30mN, and the unload process was operated by a pizeo at a speed of 0.5 μm/s. The force-distance of elastic recovery of PDMS was used to calculate the elastic modulus by related formulates of contact mechanics (Supplementary material, Eq. S1-4 and Fig. S2). The hardness of flat PDMS was measured using shore A durometer (LX-A, Shanghai Zijiu measuring tool) following "DUROMETER-A Measure of Hardness-Shore A or 00 Scale" CTM0099 (Dow Corning Corp, USA). Fig. 1c show the Shore hardness and Young modulus of PDMS with different filling ratio r.

2.4. Characterizations of wetting case on samples

Water (surface tension 71.97 mN/m), 1% sodium dodecyl sulfate solution (w/w in distilled water, surface tension 32.69 ± 0.47 mN/m, SDSS) and dimethyl silicone oil (viscosity 10 cs, surface tension 19.41 ± 0.15 mN/m) were employed here to achieve there wetting cases (non-wetting, mostly wetting and totally wetting case) (Supplementary material, Fig. S3 for liquid surface tension tests). The details characterized by the static contact angles (CAs) and spreading pictures of liquids. For CA measurements, a drops with the volume of 2 μl liquid was placed onto the sample and its image was caught by a CCD-camera. At least five measurements were performed on each sample. For the glass probe, the contact angles of water, SDSS, and silicone oil were 47.7 ± 0.5°, 10.4 ± 1.2°, ≈ 0° respectively (details are presented in Supplementary material, Fig. S5). For liquid spreading pictures, a 0.5 μl drop was placed onto the sample surface, then a digital microscope (Keyence, Japan) was used to monitor the liquid spreading.

From Fig. 2, it can be seen that the water on flat PDMS clearly exhibits non-wetting case with a static CA of about 100° and the existence of patterns produce a significant decrement in wettability, showing a hydrophobicity. For the SDSS on PDMS surfaces, it is configured as the mostly wetting case with the 0° < CA < 90°. Because of the lowest surface tension, the silicone oil on flat surface presents a nearly zero CA (Fig. 2a and S4), which means that the liquid drop can totally wet the solid showing a totally wetting case, similar to the mucus secreted by tree-frog toe-pads. Although the CA of silicone oil on hexagonal pillars is also zero, the large drop spreading map on the microscopic picture indicates that this pattern is beneficial for liquid wetting and spreading, showing an excellent drainage effect (Fig. 2b). In fact, the non-wetting and mostly wetting cases can be configured as the spreading parameter $S < 0$ ($S = [E_{subatrate}]_{dry} - [E_{subatrate}]_{wet}$) and the totally wetting case shows $S > 0$ (Gennes et al., 2004).

2.5. Adhesion measurements

Wet adhesion measurements were performed using the custom-made setup, as shown in Fig. 3a, which is also detailly described in ref. (Li et al., 2017) The probe used here is a plano-convex lens with a curve radius of 18.5 mm (Purshee, China), Young's modulus of 7.2 × 10^{11} Pa, and Poisson's ratio of 0.2. Owing to the great difference in surface tension, water, SDSS and dimethyl silicone oil were selected to achieve three different wetting cases (non-wetting case, mostly wetting case,

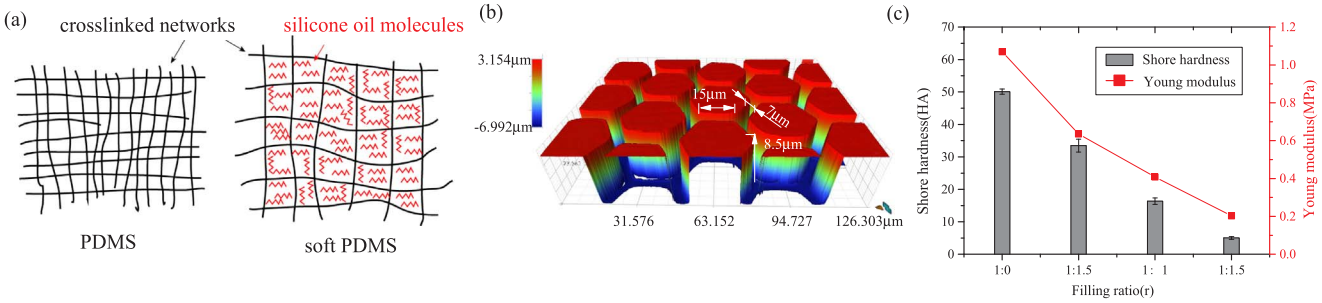

Fig. 1. (a) Schematic illustration of filling silicon oil for soft PDMS, (b) 3D profiles of the hexagonal pillars with the filling ratio r = 1.5:1, (c)shore hardness and Young modulus of flat PDMS with the silicone oil at different filling ratios to prepolymer.

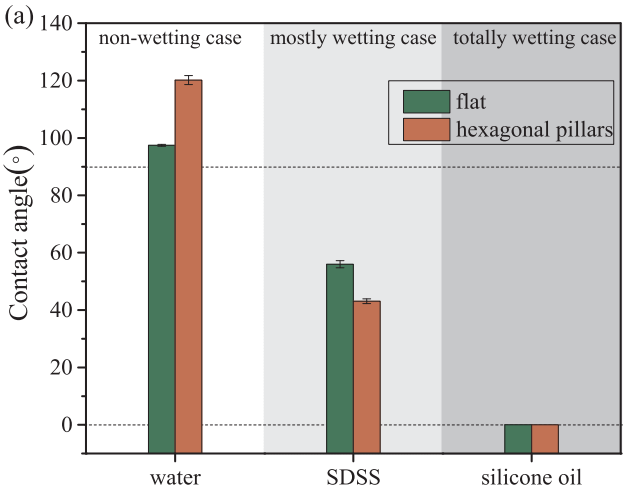

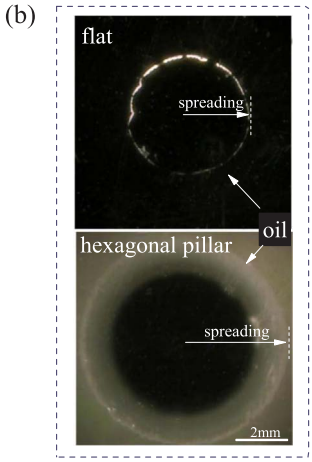

Fig. 2. (a) Contact angles measured on flat and hexagonal pillars with 3 μl liquids, (b) macroscopic spreading map of dimethyl silicone oil drop on flat and hexagonal pillars with the volume of 0.5 μl at 20 s.

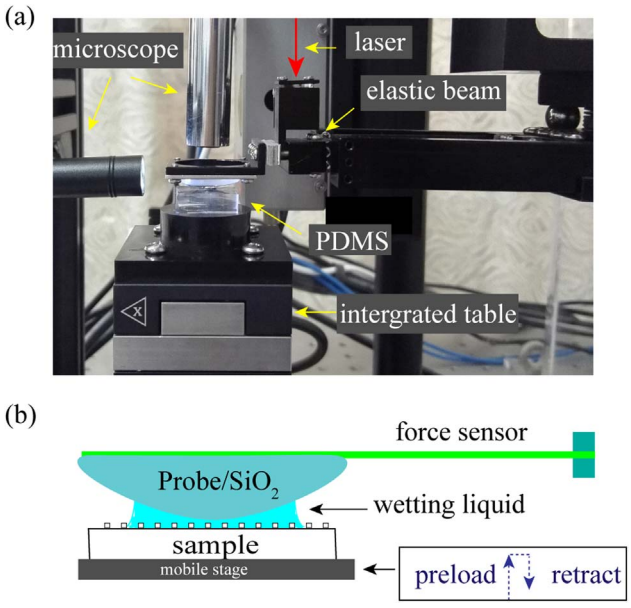

Fig. 3. (a) Optical image of the experimental setup to characterize wet adhesion properties of sample surface, (b) schematic illustration of wet measurement method.

totally wetting case) on PDMS for adhesion measurements. A 3 μl liquid was firstly placed on the samples by a micropipette, and then located the liquid drop to the center of probe under the control of microscope system. Measurements were then performed by the probe approaching, indenting, standing and retracting, as illustrated in Fig. 3b. The preload was 1 mN and the standing time was 5 s. For retractions, the piezo first moved at a speed of 1 μm/s to conduct the short-range detachment event, and when beyond the piezo range (100 μm), a step motor launched at the speed of 10 μm/s to break the long-range capillary interaction. The whole measurement process was recorded by force sensor and monitored using an optical camera. The test of each sample was at least five times. To confirm the adhesion properties of material with varying amounts of filled oil, the dry adhesion on PDMS surface was also performed. The obtained results of Fig. S6 (Supplementary material) show that the adhesion force on surface decreased with the adding of oil.

3. Results

3.1. The short- and long-range contribution for wet adhesion

Fig. 4 shows the typical adhesion force-displace curves measured on flat and hexagonal pillars with different wetting cases. A sphere-plane model with constant liquid volume for liquid bridge force was employed here to fit the capillary interaction in measured curves. The theoretical results were shown in Fig. 4 by blue dash line and its computational formula can be expressed by Butt and Kappl (2009).

$$F = 4\pi\gamma cR\left(1 - \frac{D}{\sqrt{\frac{V}{\pi R} + D^2}}\right) \text{ with } c = \frac{\cos(\theta_1 + \beta) + \cos(\theta_2)}{2} \quad (1)$$

where F is capillary force, γ is the surface tension of the liquid, R is the probe radius, β is the filling angle describing the position of the liquid meniscus, θ_1 and θ_2 are the contact angles of the liquid to the probe and the substrate, and D is the gap width. It should be noted that the real-time changes of filling angle β in testing may produce some differences to the curvature of experimental force-distance curves.

When measuring adhesion curves on flat PDMS in non-wetting case (Fig. 4a), two distinct attractive components, a drastic short-range and a smooth long-range interaction, were observed in detachment. According to the microscopy observation of obvious liquid bridges and direct contacts between probe and PDMS and the fitted theoretical capillary force value, it is evident to attributed the short-range component to direct contact forces and the long-range component to capillary forces. It was in agreement with the suggestion of early authors (Drotlef et al., 2013). In the mostly wetting case for SDSS (Fig. 4b), the detachment detected on flat PDMS gives a smooth, gentle and long force-distance curve. It indicates that no direct contact force but the long-range capillary force performs in adhesion, showing a similar condition early found between plasma treated PDMS and water (Drotlef et al., 2013). However, in a totally wetting case for silicone oil (Fig. 4c), the force-distance curve of detachment measured on flat surface shows a similar case to non-wetting case. Beside the long-range capillary part, a drastic short-range attractive interaction also performs, more obviously for hexagonal pillars (Fig. 4d). It seems that the direct contact between the PDMS and the probe happens again. Considering the fact that there is always one or several monolayers of silicone oil adsorbed on the probe and PDMS, we transform it to “close contact”, just like the case described on biological pad-epidermis (Federle et al., 2006).

3.2. The effect of wetting case on pillars’ adhesion

Fig. 5 shows adhesion forces measured on flat and hexagonal pillars

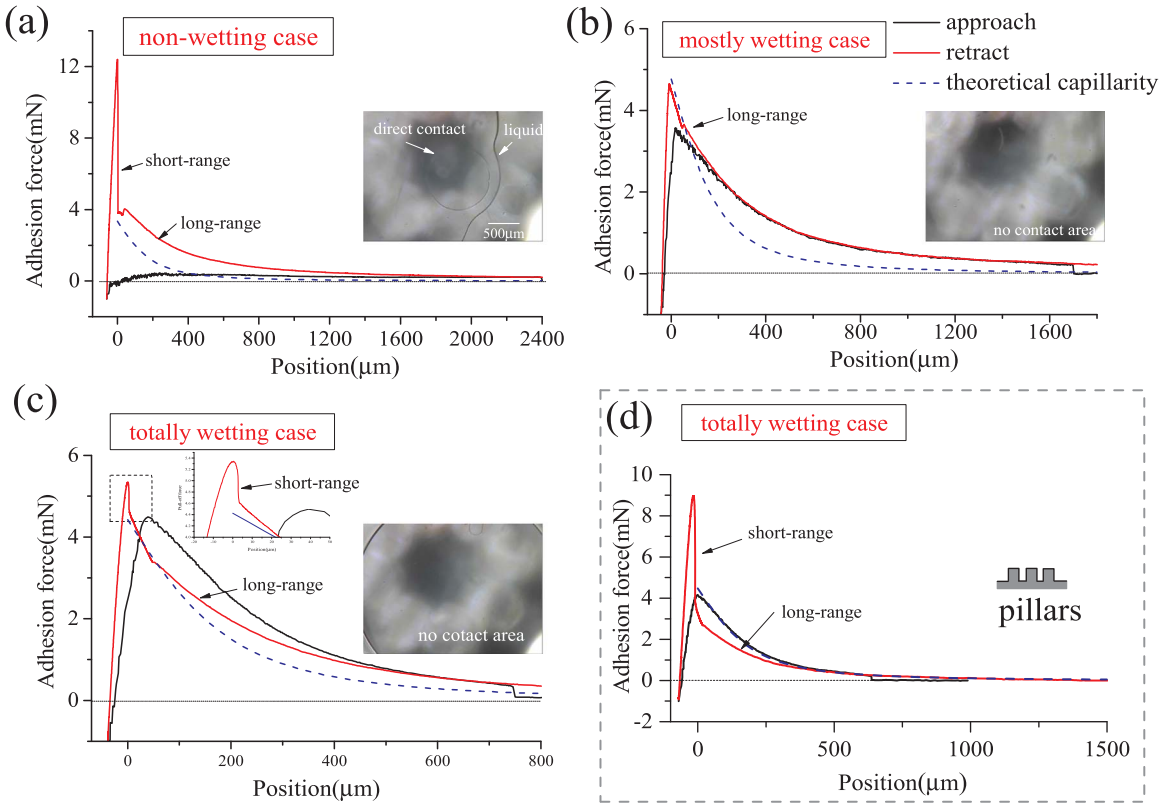

Fig. 4. Force-displacement curves recorded on flat and hexagonal pillars in different wetting cases: (a) flat with non-wetting case, (b) flat with mostly wetting case, (c) flat with totally wetting case, (d) hexagonal pillars with totally wetting case. The blue dash line represents the theoretical capillary force as a function of distance calculated with R = 18.5 mm, V = 3 μl and c = 0.2, 0.64, 0.99 (Supplementary material, Fig. S5).

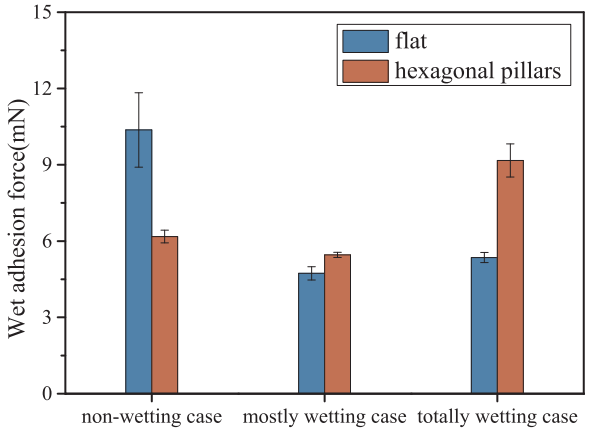

Fig. 5. Adhesion forces measured on flat and hexagonal pillars (0.203 MPa and 5 HA) in different wetting cases.

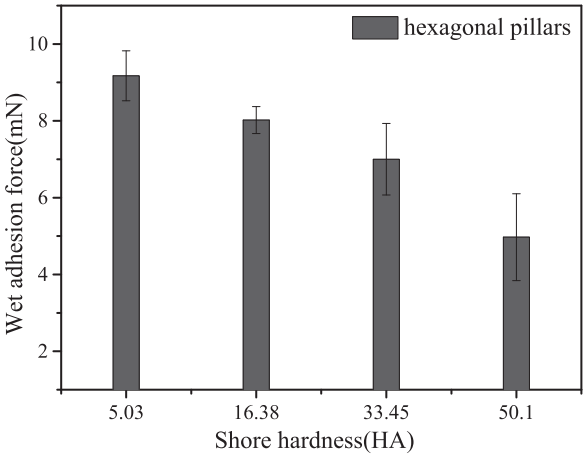

Fig. 6. Wet adhesion force of hexagonal pillar patterned surface with different softness in presence of 3 μl dimethyl silicone.

(0.203 MPa and 5 HA, the softest case) in the non-wetting, mostly wetting, and totally wetting cases. In a non-wetting case for water, the hexagonal pillar patterned surface exhibits a much lower adhesion force than that of the flat surface, presenting a similar case to dry adhesion (Supplementary material, Fig. S7). However, in the mostly wetting case for SDSS, the hexagonal pillars defeat flat surface, showing a higher adhesion force; and this enhancement in wet adhesion force was very notable in a totally wetting case for silicon oil.

3.3. The effect of softness on pillars' adhesion

Fig. 6 shows the adhesion forces of hexagonal pillar patterned surfaces with different softness measured in the presence of silicone oil (totally wetting case). It can be seen that the pull-off force in wet adhesion decreases along with the decrement of softness. The pure PDMS pillar patterned surface shows the lowest adhesion and the one with about 5 HA (Young modulus 0.203 MPa), the softest patterned surface, shows the highest adhesion. It suggests that the softer pillars are, the greater pull-off forces they behave in wet adhesion.

4. Discussion

4.1. Insights into the short-and long-range interaction

In fact, in non-wetting and mostly wetting case (S < 0, 0 < CA), the liquid on solid presented spherical cap. When a probe pressed into, the liquid would be squeezed by the deformation of soft surface, forming a

wedged film. Based on previous theories, there is a critical thickness for this film (Brochardwyart et al., 2000; Martin et al., 1997; Martinfran, Ccedil, Brochard-Wyart, 1998). The value e_c can be described as follows:

$$e_c = \sqrt{R_c|S|/E} \quad (2)$$

where R_c is the critical contact radius, S is the wedged film spreading parameter and E is elasticity modulus of PDMS. If the film is thinner than this critical value e_c, it would become metastable and an a dewetting behavior would occur induced by the nucleation caused by point-contact. The growth of dry patches leads to a direct-contact where the van der Waals force had been demonstrated to perform (Varenberg and Gorb, 2008). Note that though the distance of van der Waals interactions is less than 1 nm, but the deformation of PDMS and the slow withdrawal of crack between PDMS surface and spherical probe may lead to a large detached distance in force-distance curves (Fig. 4).

On the non-wetting case for water, because of the considerable value of $|S|$, the e_c is large (about 400 Å (Roberts and Tabor, 1968)). As a result, the dewetting may perform easily in wet adhesion where the short-range interaction of direct-contact dominates (Fig. 6a). However, on the mostly wetting case for SDSS, the repulsive electrical force between the charged monolayers of SDS molecules adsorbed on PDMS and glass probe offered resistance to the thinning of wedged film (Fig. 6b) (Roberts, 1971a; Roberts and Tabor, 1968). This resistance force was sufficient to support the normal load, forming an equilibrium film with about 200–50 Å (Roberts, 1971b; Roberts and Tabor, 1968, 1971). Because of the low parameter $|S|$, the e_c of SDSS is small, so the dewetting is difficult to be achieved by the nucleation for direct-contact (Fig. 7b). Moreover, due to the solution of an electrolyte and the thick films, the van der Waals forces can almost disappear, so only the capillary force acts in this case. Note that the repulsive electrical forces may also perform between plasma treated PDMS and glass probe, which have been used early for wet adhesion studies because of the hydroxy adsorbed both the PDMS and the glass surface.

When S > 0, i.e., a totally wetting case, the liquid on the surface spreads completely. When impressed by a probe, there will be an always stable and extremely thin film (Fig. 7c). Although this fluid thickness was not directly measured during the tests, early researchers have pointed out that for 5 cs dimethyl silicone, the wedged film between the rubber and glass gives a nearly “zero” thickness, presenting a “perfect black” contact under optical interference (Roberts and Tabor, 1968). Consequently, a close contact presumably happened here between the PDMS and the probe. Here, we can also reasonably assume that this short-range contribution was attributed to van der Waals forces interaction from two facts. First, the silicone oil is less polarizable so that when playing as a medium, it can provide a considerable Hamaker constant (Israelachvili, 2011). Then, the wedged film is very thin, probably only several monolayers thickness, which is sufficient for Van der Waals interactions. These findings also coincide with the previous suggestion by Barnes that van der Waals forces may perform in the close contact of tree-frog adhesion (Barnes, 2012).

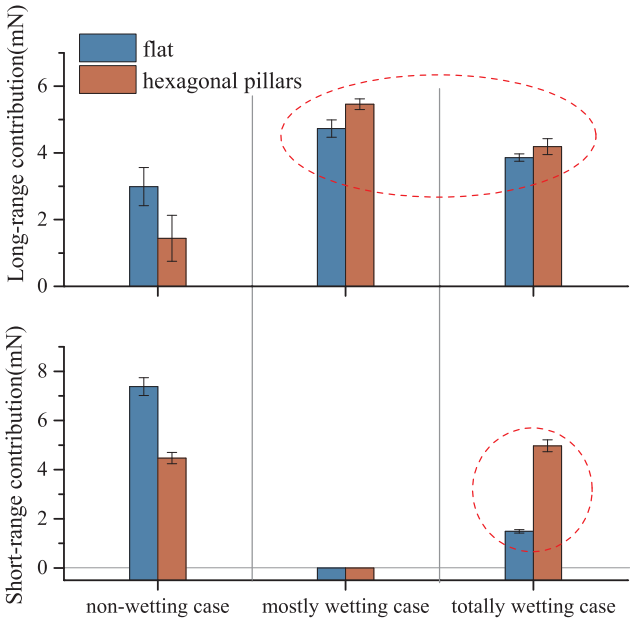

Fig. 8. Long- and short-range contributions of wet adhesion on flat and hexagonal pillars in different wetting cases.

4.2. The effect of wetting case on pillars’ adhesion

To reveal the adhesion mechanism of pillars in different wetting cases, the wet adhesion forces were divided into two attractive parts (Fig. 8), i.e. the short- and long-range contribution, based on raw force-distance curves. It is clear that in the non-wetting case (CA > 90°), the short-range direct contact components play a leading role and the long-range capillary components behave as a secondary one. The direct contact component was strongly weakened by the micro-pillars due to the decreased contact area between the probe and PDMS. Meanwhile, the high repulsion to water of patterns (showing high CAs, Fig. 2a) also decreased the long-range capillary contributions in wet adhesion. As a consequence, we assume that the hexagonal pillars are in disadvantage in adhesion with a non-wetting liquid. When in the mostly wetting case (0° < CA < 90°), the wet adhesion was thoroughly dominated by the long-range capillary force caused by a single liquid bridge whose contact line was expanded by the presence of an “open” pattern through its

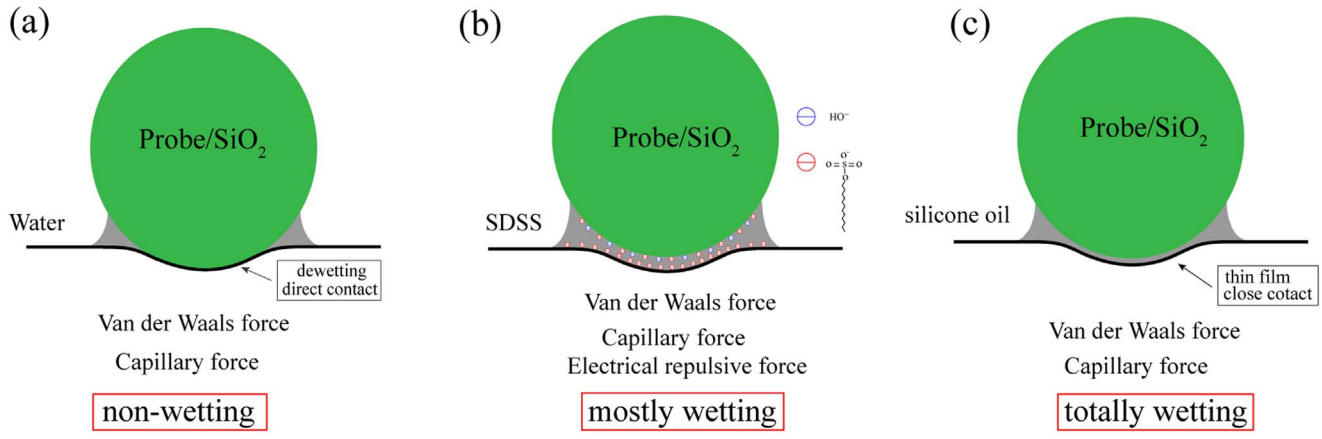

Fig. 7. Illustration of adhesion mechanism between the probe and flat PDMS in different wetting cases.

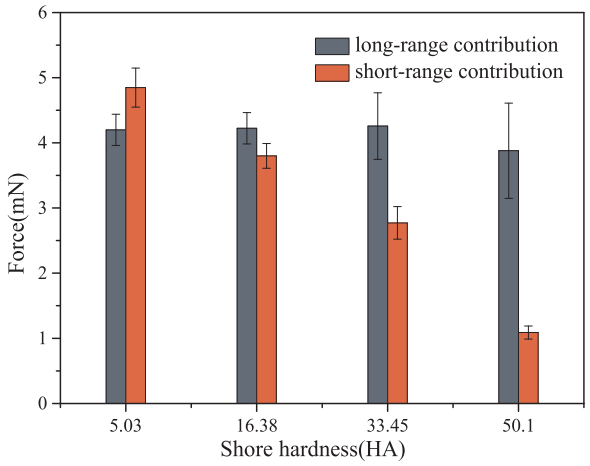

Fig. 9. Short- and long-range contribution of hexagonal pillar patterned surface with different softness in presence of 3 μl dimethyl silicone.

excellent liquid spreadability and wetting power. The hexagonal pillars, therefore, presented a larger wet adhesion force than flat. In a totally wetting case (CA = 0°), the short-range contribution induced by "close contact" of hexagonal pillars is higher than the one of flat in wet adhesion. We attribute it to its drainage effect can possibly further lower the film (Fig. 2b), producing a closer contact between the probe and PDMS, where van der Waals forces perform strongly. For the long-range capillary forces, hexagonal pillars behave similarly to mostly wetting case.

4.3. The effect of softness on pillars' adhesion

Similarly, according to the raw force-displacement curves, the wet adhesion data of Fig. 6 has also been divided into two components, the short- and long-range attractive contribution (Fig. 9). For the long-range contributions, the interacted values measured on patterned surfaces with different softness show little difference. On the contrary, for the short-range ones, they were weakened by the decreased softness on hexagonal pillars. Based on previous suggestions, the long-range contribution here is driven by the capillary force caused by a liquid bridge, so it is difficult to be influenced by the softness of patterns. On the contrary, the short-range contributions are caused by "close contact" which means that the closer and the larger area the probe contacts, the more drastic detachment achieves. As a result, the softness of hexagonal patterns can play a beneficial role in wet adhesion due to the enhanced drainage effects and the large contact area caused by the ductile property.

5. Conclusion

In this paper, very soft bioinspired hexagonal pillars are fabricated using filling low viscosity silicone oil into PDMS. Their adhesion behaviors in the non-wetting, mostly wetting and totally wetting cases are evaluated and compared to unpatterned surfaces.

In a totally wetting case (dimethyl silicone), i.e. a biological toe-pad-like case, our results suggest that besides the long-range capillary forces, a short-range contribution caused by "close contact" can also play a significant role for wet adhesion force. Compared with unpatterned surfaces, the hexagonal pillar designs can highlight both the short-range and long-range interaction for wet adhesion with their excellent drain effects. Moreover, the softness of microstructure can effectively enhance the short-range interaction for wet adhesion.

In a non-wetting case (water), the dewetting behaviors happen between the probe and PDMS. The wet adhesion forces depend more heavily on the short-range direct contact forces than capillary interactions. Due to the decreased contact area to probe and the increased repulsion to water, the hexagonal pillar design is disadvantage for wet adhesion.

In a mostly wetting case (SDSS), because of the resistance of repulsive electrical forces, only the capillary forces dominate the wet adhesion and the hexagonal pillars are beneficial for wet adhesion with their enlarged spreading areas of solid/liquid.

Acknowledgements

This research was supported by the National Nature Science Foundation of China (NSFC) (Grant no. 51675268) and the Fundamental Research Funds for the Central Universities (Grant NZ2016106).

Appendix A. Supporting information

Supplementary data associated with this article can be found in the online version at http://dx.doi.org/10.1016/j.jmbbm.2017.11.036.

References

Barnes, W.J., Baum, M., Peisker, H., Gorb, S.N., 2013. Comparative Cryo-SEM and AFM studies of hylid and rhacophorid tree frog toe pads. J. Morphol. 274, 1384–1396.
Barnes, W.J., Oines, C., Smith, J.M., 2006. Whole animal measurements of shear and adhesive forces in adult tree frogs: insights into underlying mechanisms of adhesion obtained from studying the effects of size and scale. J. Comp. Physiol. A 192, 1179–1191.
Barnes, W.J.P., 1999. Tree frogs and tire technology. Tire Technol. Int. 99, 42–47.
Barnes, W.J.P., 2007. Functional morphology and design constraints of smooth adhesive pads. MRS Bull. 32, 479–485.
Barnes, W.J.P., 2012. Adhesion in Wet Environments: Frogs. Springer, Netherlands.
Barnes, W.J.P., Goodwyn, P.J.P., Nokhbatolfoghahai, M., Gorb, S.N., 2011. Elastic modulus of tree frog adhesive toe pads. J. Comp. Physiol. A 197, 969–978.
Barnes, W.J.P., Smith, J., Oines, C., Mundl, R., 2002. Bionics and wet grip. Tire Technol. Int. 2002, 56–60.
Brochardwyart, F., Buguin, A., Martin, P., Martin, A., Sandre, O., 2000. Adhesion of soft objects on wet substrates. J. Phys. Condens. Matter 12, A239–A244.
Butt, H.J., Kappl, M., 2009. Normal capillary forces. Adv. Colloid Interface Sci. 146, 48–60.
Drotlef, D.M., Appel, E., Peisker, H., Dening, K., del Campo, A., Gorb, S.N., Barnes, W.J.P., 2014. Morphological studies of the toe pads of the rock frog, Staurois parvus (family: Ranidae) and their relevance to the development of new biomimetically inspired reversible adhesives. Interface Focus 5 (20140036-20140036).
Drotlef, D.M., Stepien, L., Kappl, M., Barnes, W.J.P., Butt, H.J., del Campo, A., 2013. Insights into the adhesive mechanisms of tree frogs using artificial mimics. Adv. Funct. Mater. 23, 1137–1146.
Endlein, T., Barnes, W.J.P., Samuel, D.S., Crawford, N.A., Biaw, A.B., Grafe, U., 2013. Sticking under wet conditions: the remarkable attachment abilities of the torrent frog, Staurois guttatus. PLoS One 8, e73810.
Federle, W., Barnes, W.J., Baumgartner, W., Drechsler, P., Smith, J.M., 2006. Wet but not slippery: boundary friction in tree frog adhesive toe pads. J. R. Soc. Interface 3, 689–697.
Fischer, S.C.L., Levy, O., Kroner, E., Hensel, R., Karp, J.M., Arzt, E., 2016. Bioinspired polydimethylsiloxane-based composites with high shear resistance against wet tissue. J. Mech. Behav. Biomed. Mater. 61, 87–95.
Gennes, P.G.D., Brochard-Wyart, F., Quéré, D., 2004. Capillarity and Wetting Phenomena. Springer, New York.
Green, D.M., 1979. Treefrog toe pads: comparative surface morphology using scanning electron microscopy. Can. J. Zool. 57, 2033–2046.
Green, D.M., Simon, M.P., 1986. Digital microstructure in ecologically diverse sympatric microhylid frogs, genera cophixalus and sphenophryne (Amphibia, Anura), from Papua-New-Guinea. Aust. J. Zool. 34, 135–145.
Hanna, G., Barnes, W.J.P., 1991. Adhesion and detachment of the toe pads of tree frogs. J. Exp. Biol. 155, 103–125.
Huang, W., Wang, X.L., 2013. Biomimetic design of elastomer surface pattern for friction control under wet conditions. Bioinspiration Biomim. 8, 046001.
Israelachvili, J.N., 2011. Intermolecular and Surface Forces: Revised, third ed. Academic press.
Iturri, J., Xue, L., Kappl, M., García-Fernández, L., Barnes, W.J.P., Butt, H.J., del Campo, A., 2015. Torrent frog-inspired adhesives: attachment to flooded surfaces. Adv. Funct. Mater. 25, 1499–1505.
Li, M., Huang, W., Wang, X., 2015. Bioinspired, peg-studded hexagonal patterns for wetting and friction. Biointerphases 10, 031008.
Li, M., Huang, W., Wang, X., 2017. Advanced adhesion and friction measurement system. Meas. Sci. Technol. 28, 035601.
Lorenz, B., Persson, B.N., 2011. Fluid squeeze-out between rough surfaces: comparison of theory with experiment. J. Phys. Condens. Matter.: Inst. Phys. J. 23, 355005.
Martin, P., P. Silberzan, A., Brochardwyart, F., 1997. Sessile droplets at a solid/elastomer interface. Langmuir: ACS J. Surf. Colloids 13, 4910–4914.

Martinfran, Ccedil, P., Brochard-Wyart, O., 1998. Dewetting at soft interfaces. Phys. Rev. Lett. 80, 3296–3299.
Persson, B.N.J., 2007. Wet adhesion with application to tree frog adhesive toe pads and tires. J. Phys. Condens. Mat. 19, 376110.
Roberts, A., 1971a. Role of electrical repulsive forces in synovial fluid. Nature 231, 434–436.
Roberts, A.D., 1971b. Squeeze films between rubber and glass. J. Phys. D. Appl. Phys. 4, 423–432.
Roberts, A.D., Tabor, D., 1968. Surface forces: direct measurement of repulsive forces due to electrical double layers on solids. Nature 219, 1122.
Roberts, A.D., Tabor, D., 1971. The extrusion of liquids between highly elastic solids. Proc. R. Soc. A Math. Phys. Eng. Sci. 325, 323–345.
Roshan, R., Jayne, D.G., Liskiewicz, T., Taylor, G.W., Gaskell, P.H., Chen, L., Montellano-Lopez, A., Morina, A., Neville, A., 2011. Effect of tribological factors on wet adhesion of a microstructured surface to peritoneal tissue. Acta Biomater. 7, 4007–4017.
Scholz, I., Barnes, W.J., Smith, J.M., Baumgartner, W., 2009. Ultrastructure and physical properties of an adhesive surface, the toe pad epithelium of the tree frog, Litoria caerulea White. J. Exp. Biol. 212, 155–162.
Varenberg, M., Gorb, S.N., 2008. A beetle-inspired solution for underwater adhesion. J. R. Soc. Interface 5, 383–385.
Varenberg, M., Gorb, S.N., 2009. Hexagonal surface micropattern for dry and wet friction. Adv. Mater. 21, 483–486.
Wang, S., Li, M., Huang, W., Wang, X., 2016. Sticking/climbing ability and morphology studies of the toe pads of Chinese fire belly newt. J. Bionic Eng. 13, 115–123.